Dalton Transactions

ROYAL SOCIETY OF CHEMISTRY

PAPER

View Article Online
View Journal

Cite this: DOI: 10.1039/d1dt01455b

A simple strategy for the visual detection and discrimination of Hg^{2+} and CH_3Hg^+ species using fluorescent nanoaggregates†

Nilanjan Dey [a,b]

Fluorescent nanoaggregates (FNAs) based on phenanthroline-based amphiphiles show changes in solution color from colorless to yellow upon addition of both Hg^{2+} (LOD ~4 ppb) and CH_3Hg^+ (LOD ~18 ppb). However, the extent of fluorescence quenching is more prominent with Hg^{2+} (~12 fold) than with CH_3Hg^+ (~4 fold). Also, unlike Hg^{2+}, the interaction of CH_3Hg^+ needs more time, ~10 min at room temperature. Experimental evidence indicates that both mercury species coordinate with the phenanthroline unit and facilitate the charge transfer interaction while destabilizing the nanoassembly. The lower charge density on CH_3Hg^+ along with its large size compared to Hg^{2+} may be the reason for such observations. Interestingly, FNAs show a selective response towards CH_3Hg^+ when pre-treated with EDTA. Further, analysis of heavy metal pollutants in drinking water and biological samples was performed. High recovery values ranging from 96% to 103.0% were estimated along with relatively small standard deviations (<3%). Low-cost, reusable test strips were designed for rapid, on-site detection of mercury species. Further, the *in situ* formed metal complexes are allowed to interact with thiol-containing amino acids. As expected, CH_3Hg^+, being less thiophillic, endures less interaction with cysteine. Mechanistic investigations indicate that thiolated amino acids can bind with the metal ion center and form a tertiary complex (cooperative interaction).

Received 3rd May 2021,
Accepted 27th May 2021

DOI: 10.1039/d1dt01455b

rsc.li/dalton

Introduction

Environmental pollution caused by heavy metal and metalloids, such as mercury, arsenic, cadmium, iron, copper, nickel, and lead (density >5 gm cm^{-3}), has become a global concern due to their adverse effects on human health and well-being.[1] Although some of these metal ions play important roles in several physiological processes and proper functioning of enzymes, their excess accumulation in the body can cause damage to one or more essential organs, resulting in severe health problems and even death.[2] Lately, optical probes have been involved extensively in the analysis of real-life samples due to their structural diversity, low maintenance cost, high sensitivity, simple protocols, and quick response times.[3] Among them, ratiometric colorimetric probes are of particular interest because they can detect toxic pollutants by the naked eye with little to no background interference. Although there are numerous reports on colorimetric sensing of Hg^{2+} ions, optical probes for CH_3Hg^+ are very few in number.[4] However, methylmercury compounds are known to be more toxic to living organisms than the inorganic forms of mercury. Due to their superior lipid solubility, methylmercury species can easily cross biological membranes, including the blood–brain barrier, and deposit in different internal organs, such as the brain, kidneys and nerve system.[5] Exposure to CH_3Hg^+ even at a lower concentration can cause prenatal brain damage, cognitive and motion disorders, and vision and hearing loss, while excess intake results in Minamata disease.[6] Owing to its less thiophilic nature and lower charge compared to Hg^{2+}, CH_3Hg^+ species generally yield a slower response and require larger amounts to receive a detectable optical signal.[7]

Additionally, it has been observed that depending upon their size, charge density, coordination behavior and crystal field stabilization energy, metal ions can bind with various biomolecules, such as nucleotides, amino acids, proteins, enzymes, and anions.[8] For example, affinity of Ni^{2+} to histidine has often been utilized for purifying histidine-tagged protein molecules.[9] Similarly, metal complexes based on Cu^{2+} or Zn^{2+} are regularly used for selective extraction of phosphorylated proteins and peptides.[10]

Considering these facts, herein, we have reported the detection as well as the differentiation of inorganic (Hg^{2+}) and organic mercury species (CH_3Hg^+) using fluorescent nanoag-

[a]Graduate School of Science, Kyoto University, Sakyo, Kyoto 606-8502, Japan. E-mail: nilanjan@hyderabad.bits-pilani.ac.in
[b]Department of Chemistry, BITS-Pilani Hyderabad Campus, Shameerpet, Hyderabad-500078, Telangana, India

†Electronic supplementary information (ESI) available. See DOI: 10.1039/d1dt01455b

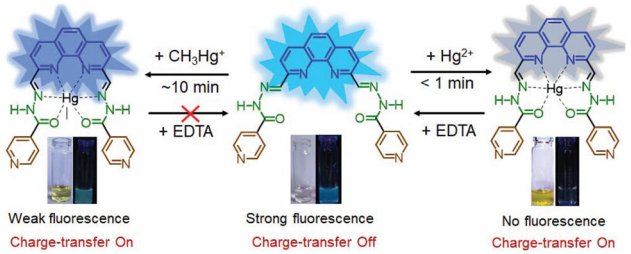

Scheme 1 Schematic showing differential response towards inorganic (Hg^{2+}) and organic (CH_3Hg^+) mercury species.

gregates (Scheme 1) composed of phenanthroline-based amphiphiles. Both CH_3Hg^+ and Hg^{2+} could result in changes of the solution color from colorless to yellow. However, unlike Hg^{2+}, CH_3Hg^+ needs a ~10 min resting time. Also, the extent of fluorescence quenching was found to be more prominent for Hg^{2+} than for CH_3Hg^+. Interestingly, the compound could show a specific interaction with CH_3Hg^+ when pre-treated with EDTA. Further, we utilized the present system to analyze both Hg^{2+} and CH_3Hg^+ species in natural water samples (important for waste-water management), in the presence of plasma proteins (important in clinical diagnosis), *etc*. Low-cost, reusable paper strips were designed for rapid, on-site detection of possible contamination. Further, the *in situ* formed metal complexes have been involved in probing sulfhydryl-containing amino acids, such as cysteine and homocysteine. Mechanistic investigations indicate that the amino acids can bind (cooperatively) to the metal complex *via* thiol units and destabilize the charge-transfer state.

Results and discussion

Design and synthesis of the optical probe

Compound **1** was synthesized by following a literature-reported protocol *via* the carbonyl-nucleophilic addition reaction of 1,10-phenanthroline-2,9-dicarbaldehyde with isoniazid. The compound could form a pH-dependent, thermosensitive nano assembly in aqueous medium.[11] Thus, a broad, red-shifted fluorescence band (λ_{max} = 465 nm, Φ = 0.14) was observed at pH 7.0 in PBS buffer. The presence of residual absorbance in a longer wavelength region in the UV-visible spectrum also supported this assumption (Fig. S1†). Although nanoaggregates of **1** have already been reported, we independently proved the assembly formation *via* dynamic light scattering and transmission electron microscopic studies (Fig. 1a and 3a). Considering the affinity of the phenanthroline moiety towards transition metal ions, we could anticipate that **1** would be a good candidate for analyzing heavy metal pollutants (Fig. 1b).[12] However, the presence of acyl hydrazone units on both sides of the phenanthroline unit is expected to modify the metal ion binding efficiency of **1**. Unlike in THF medium, compound **1** showed a broad, structureless excitation spectrum (at 454 nm) in PBS buffer (pH 7.0), presumably due to the self-assembly formation (Fig. S2†). Also, the absorption

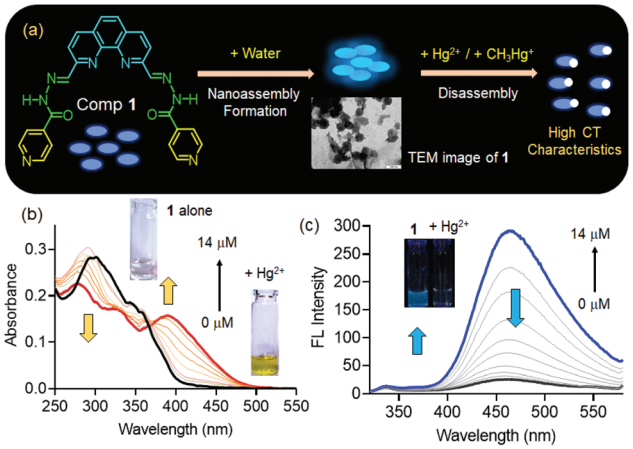

Fig. 1 (a) Schematic showing Hg^{2+}/CH_3Hg^+-induced disassembly of nanoaggregates of **1** (a TEM image of **1** is shown in the middle). (b) UV-visible titration of **1** (10 μM) with Hg^{2+} at pH 7.0 in PBS buffer. (c) Fluorescence titration of **1** (10 μM, λ_{ex}: 320 nm) with Hg^{2+} at pH 7.0 in PBS buffer.

spectra showed a very small hypsochromic shift even when exposed to UV radiation for ~30 min (365 nm, 300 mW cm^{-2}). This suggests fairly high photostability of the fluorescent nanoaggregates (Fig. S3†).

Interaction with inorganic mercury at biological pH

In aqueous medium, compound **1** showed a change in solution color from colorless to yellow selectively in the presence of Hg^{2+}. As expected, the UV-visible spectrum showed the appearance of a new red-shifted charge-transfer band at ~420 nm upon the addition of Hg^{2+} ion. However, no change in solution color or in the UV-visible spectra was observed when other divalent or trivalent metal ions were added under similar conditions (Fig. 2a). The concentration-variation studies with Hg^{2+} ion showed a gradual increase in absorbance in the ~420 nm region with a concomitant decrease at ~310 nm (ratiometric response) (Fig. 1c and S4†). The Job's plot analysis confirms 1 : 1 binding stoichiometry with an inflection point at X = 0.5 (X = molar ratio of **1** and Hg^{2+}) (Fig. 2b). The titration studies also indicate that **1** can detect as low as 4.2 ppb Hg^{2+} in aqueous medium. The affinity constant ($\log K$) was estimated as 4.47 ± 0.03 based on the 1 : 1 molecular model (Fig. S1b†).[13] The formation of such thermodynamically stable Hg^{2+}-complexes with phenanthroline ligands has been reported earlier.[14]

pH-Variation studies revealed that the binding of **1** with Hg^{2+} occurred effectively over a wide range of pH from 4.5 to 9 (Fig. 2c). We suspected that protonation at the phenanthroline nitrogen ends below pH 4.5 might resist further interaction with Hg^{2+}. Because real-life samples are often tainted by the presence of multiple toxic ions, we also examined the response of **1** towards Hg^{2+} ion in the presence of other competitive metal ions (Fig. S5†). However, no significant change in optical response was observed when Hg^{2+} ion was mixed with other metal ions, even at excess concentrations.

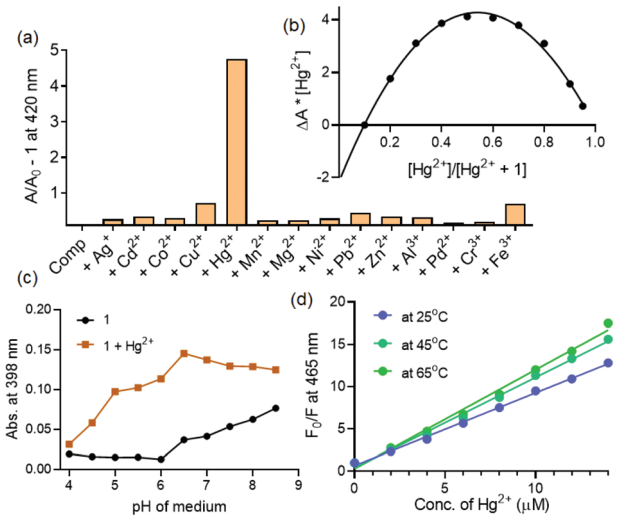

Fig. 2 (a) Change in absorbance of **1** (10 μM) upon addition of different metal ions (15 μM) at pH 7.0 in PBS buffer. (b) Job's plot analysis of **1** with Hg^{2+} at pH 7.0 in PBS buffer. (c) Effect of pH on the interaction of **1** (10 μM, λ_{ex}: 320 nm) with Hg^{2+} (15 μM). (d) Effect of temperature on the interaction of **1** (10 μM, λ_{ex}: 320 nm) with Hg^{2+} (0–14 μM).

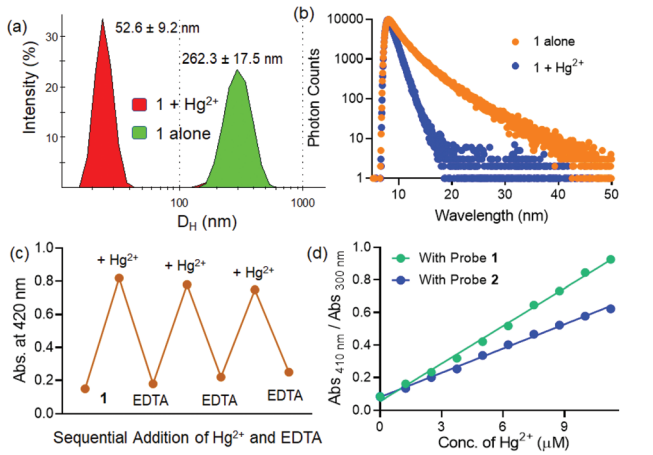

Fig. 3 (a) Hydrodynamic diameter (D_H) of **1** (10 μM) upon addition of Hg^{2+} (15 μM) at pH 7.0 in PBS buffer. (b) Fluorescence decay profile of **1** (10 μM, λ_{ex}: 320 nm, λ_{em}: 465 nm) with Hg^{2+} (15 μM) at pH 7.0 in PBS buffer. (c) Recovery experiment with EDTA showing the reversible interaction of **1** (10 μM) with Hg^{2+} (15 μM). (d) Comparison of the interactions of **1** and **2** (10 μM) with Hg^{2+} at pH 7.0 in PBS buffer.

Rationalization of binding interaction

Under a long UV lamp, **1** showed cyan-colored FL, as evidenced by the formation of a fluorescence band at ~465 nm. Among various transition metal ions, only Hg^{2+} ion induced a ~15 nm blue shift in the FL maximum along with ~12-fold quenching in intensity (Fig. 1d). These observations indicate the possibility of Hg^{2+}-induced dissociation of the preformed nanoassembly (Fig. 3a).[15] The high spin–orbit coupling constant of Hg^{2+} could also be the contributing factor.[16] To confirm this, we performed dynamic light scattering studies both with and without Hg^{2+} ion. As anticipated, a reduction in the average hydrodynamic diameter of the aggregates could be seen upon the addition of Hg^{2+}. On the other hand, temperature-dependent quenching studies with Hg^{2+} showed an increment in Stern–Volmer constant values at a higher temperature, indicating the dynamic nature of the quenching process (Fig. 2d). A reduction in average FL lifetime value was noticed when **1** was treated with Hg^{2+}, presumably due to dissociation of the aggregated structure (Fig. 3b). Because it is known in the literature that transition metal ions, such as Cu^{2+}, Fe^{3+}, and Hg^{2+}, can either form a coordination complex or become involved in the hydrolysis of acyl hydrazone units.[17] The EDTA-mediated recovery experiment suggests that the observed change in the UV-visible spectrum with Hg^{2+} is reversible, indicating no possibility of an ion-induced hydrolysis reaction (Fig. 3c).

Further, the ^{1}H-NMR titration of **1** with Hg^{2+} (0–1 equiv.) was performed in DMSO-d_6/D_2O (1 : 1) mixture medium to comment on the mode of binding (Fig. S6†). The titration studies reveal broadening of the NMR signals along with prominent downfield shifts. The extents of the downfield shifts were more prominent for the protons adjacent to the imine functional group and phenanthroline nitrogen ends. Thus, we might conclude that in the present scenario, the Hg^{2+} ion is binding to the phenanthroline site rather than the pyridine units. The formation of the 1 : 1 complex was also evident from the ESI-MS mass spectral analysis (Fig. S7†). To verify the involvement of the pyridine end, we performed the experiment with another compound (**2**) without pyridyl ends. The control compound showed interaction with Hg^{2+}, but to a lesser extent (Fig. 3d). This apparent discrepancy can be attributed to the differences in the electronic characteristics of the acylhydrazone units.

Interaction with organic mercury species (CH_3Hg^+)

When **1** was exposed to CH_3Hg^+, the formation of a yellow-colored solution was noted. Here, we also witnessed the appearance of the CT band in the ~410 nm region. However, unlike Hg^{2+}, here, the response time was considerably slow; ~10 min incubation time was required (Fig. 4d). Titration experiments of **1** with CH_3Hg^+ were carried out under similar conditions to that of Hg^{2+}. The UV-visible titration studies showed that ~7 equiv. CH_3Hg^+ (~5-fold larger than Hg^{2+}) were needed for saturation of the optical signal (Fig. 4a). On the other hand, the extent of fluorescence quenching was found to be less prominent compared to inorganic mercury species, *i.e.* Hg^{2+} (Fig. 4b). Unlike Hg^{2+}, here, ~4-fold quenching of the FL intensity was observed upon addition of CH_3Hg^+. In this case, the Job's plot analysis also indicates 1 : 1 binding stoichiometry (Fig. S8a†). The affinity constant was calculated as 3.88 ± 0.02 by fitting the data with the Benesi–Hildebrand 1 : 1 binding equation (Fig. S8b†). Also, titration studies indicate that the minimum detectable concentration is 18.2 ppb for CH_3Hg^+ species.

Although the FL response of CH_3Hg^+ was found to be very similar to that of Hg^{2+}, no change in absorbance was noticed when EDTA was added to the aqueous solution of **1** + CH_3Hg^+

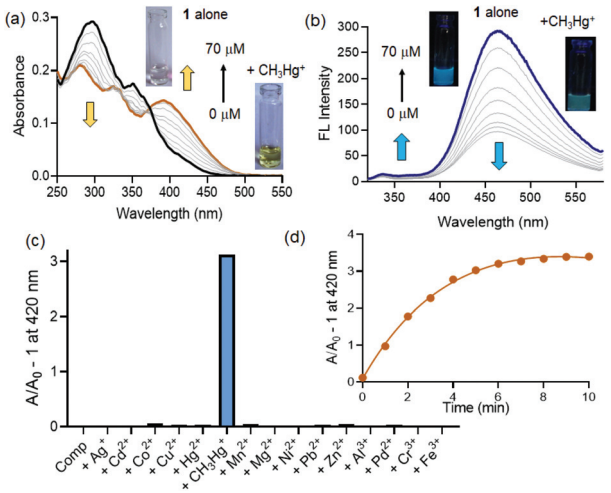

Fig. 4 (a) UV-visible titration of **1** (10 μM) with CH_3Hg^+ at pH 7.0 in PBS buffer. (b) Fluorescence titration of **1** (10 μM, λ_{ex}: 320 nm) with CH_3Hg^+ at pH 7.0 in PBS buffer. (c) Changes in absorbance of **1** (10 μM) with different metal ions (70 μM) in the presence of EDTA (0.1 mM). (d) Time-dependent changes in absorbance with CH_3Hg^+ (70 μM) at pH 7.0 in PBS buffer.

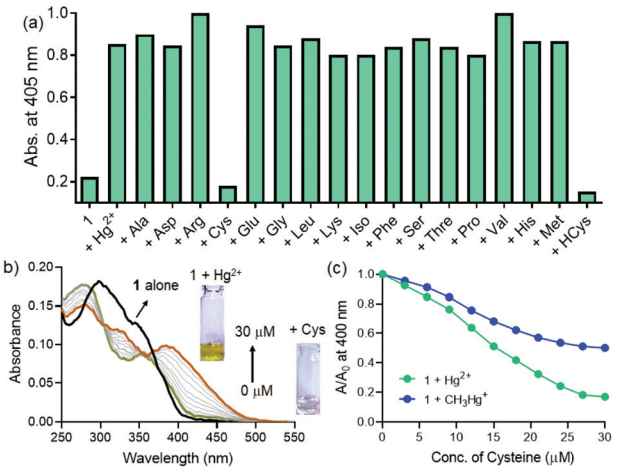

Fig. 5 (a) Change in absorbance of **1** + Hg^{2+} (10 μM, 1 : 1) with different amino acids (30 μM) at pH 7.0 in PBS buffer. (b) UV-visible titration of **1** + Hg^{2+} (10 μM, 1 : 1) with cysteine at pH 7.0 in PBS buffer (the inset shows images of vials with and without cysteine). (c) Interaction of **1** + Hg^{2+} and **1** + CH_3Hg^+ with cysteine through cooperative binding.

(Fig. S9a†). Unlike Hg^{2+}, EDTA was not able to remove CH_3Hg^+ from the complex. This is quite expected, as it is known that the binding affinity of EDTA for CH_3Hg^+ is 10^{16} times weaker than that for Hg^{2+}.[18] Based on this observation, we could develop a selective colorimetric assay for CH_3Hg^+ using a mixture of **1** and EDTA as a probe. After pretreatment with EDTA, no other metal ions (including Hg^{2+}) except CH_3Hg^+ could induce the formation of the charge transfer band (Fig. 4c). Thus, the present system can detect and distinguish both organic (CH_3Hg^+) and inorganic mercury (Hg^{2+}) species.

Tandem sensing of amino acids at biological pH

Considering the thiophilic nature of Hg^{2+} ion, we exploited the *in situ* generated metal complex to analyze thiol-containing amino acids, such as cysteine and homocysteine. To accomplish this, a mixture solution of **1** and Hg^{2+} in a 1 : 1 ratio was freshly made and equilibrated for ~30 min before the studies. The addition of sulfhydryl-containing amino acids turned the yellow solution colorless. The UV-visible spectral studies indicate that the CT signal at ~410 nm almost disappeared in the presence of these amino acids with the formation of two new bands at 280 and 352 nm, respectively (Fig. 5b and S9b, S10†). In both cases, the titration reached saturation with the addition of only 2 equivalents of the target amino acids. No amino acids, other than cysteine and homocysteine, induced detectable changes in the absorbance (Fig. 5a). A similar type of spectral change was observed when an aqueous solution of **1** + CH_3Hg^+ was exposed to cysteine. However, the extent of the change was less prominent than that of Hg^{2+}. This may be due to the poor thiophilicity of the CH_3Hg^+ species as compared to Hg^+ (Fig. 5c). On the other hand, addition of both cysteine and homocysteine to **1** + Hg^{2+} resulted in a turn-on FL response (at 450 nm) (Fig. S11†). To verify whether the interaction of amino acids (cysteine, homocysteine, *etc.*) is independent of Hg^{2+} binding, we performed a Hill plot analysis. The positive Hill coefficient values indicate cooperative binding of amino acids in both cases (Fig. 6a and S12†).[19]

Rationalization of amino acid binding

Because probe **1** alone did not show any interaction with either cysteine or homocysteine, it can be assumed that the amino acids are interacting with the metal complex through Hg^{2+} ion (Fig. S13a†). In general, amino acids can either form a ternary adduct with an *in situ* formed metal complex or dis-

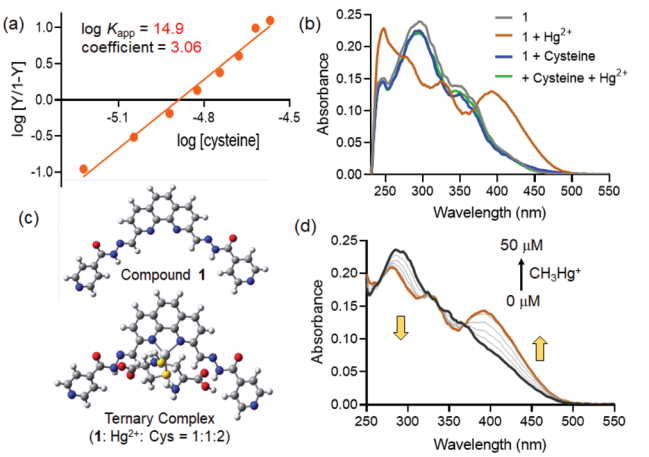

Fig. 6 (a) Hill-plot analysis showing the cooperative interaction with cysteine in water (pH 7.0). (b) Reversibility check by sequential addition of Hg^{2+} (15 μM) and cysteine (30 μM) in water (pH 7.0). (c) Energy-minimized structures of **1** and the tertiary complex with Hg^{2+} and cysteine. (d) UV-visible titration of **1** (10 μM) with CH_3Hg^+ (0–50 μM) at pH 7.0 in PBS buffer (with ~0.1 mg mL^{-1} HSA).

sociate the preformed metal complex by forming a thermodynamically more stable alternative complex with metal ions.[20] The sequential addition of Hg^{2+} and cysteine in the same solution showed no recovery of the spectrum of native **1**, which ruled out the possibility of a reversible interaction (displacement approach) between the metal complex and cysteine (Fig. 6b). Although the absorption spectrum of **1** + Hg^{2+} upon treatment with cysteine did not show a similar CT band to **1** alone, the UV-visible spectra appeared to be quite different. These differences again dismiss the idea of the release of 'free' probe during the interaction with amino acids. The ^{1}H NMR titration of **1** + Hg^{2+} with cysteine showed regeneration of the peaks, but at different positions with different splitting patterns (Fig. S13b†). Thus, we may assume that the species generated in the reaction medium is not free probe but a ternary complex with reduced charge transfer characteristics. The ESI-MS spectrum of **1** + Hg^{2+} in the presence of both cysteine and homocysteine indicates the formation of a ternary complex with 1 : 1 : 2 stoichiometry (Fig. S14 and S15†).

Density functional calculations using the B3LYP/6-31G* level of theory showed that in the energy-minimized structure of **1** + Hg^{2+}, the metal ion binds to the phenanthroline and imine nitrogen ends (Fig. S16†).[21] On the other hand, the ternary composite [1 : 1 : 2 for compound **1** : Hg^{2+} : cysteine] with cysteine showed a tetrahedral coordination site for Hg^{2+} ion, comprised of two nitrogen ends of the phenanthroline unit and sulfhydryl groups of two coordinated cysteine molecules (Fig. 6c). The Hg–N bond lengths were found to be 2.08 and 2.10 Å, while the Hg–S bond lengths were 2.49 and 2.47 Å, respectively.

Application in real-life sample analysis

Analysis of biological samples. Determination of CH_3Hg^+ or Hg^{2+} in blood or urine samples of hospitalized people is essential to confirm a diagnosis of poisoning or to assist in forensic investigation. However, these biological fluids mostly contain serum albumin (HSA) protein in large excess.[22] Thus, to achieve a quantitative estimation of mercury species in biological fluids, it is essential that the sensor molecule show interaction with the analytes even in presence of excess HSA. To confirm this, we repeated the titration of **1** with both Hg^{2+} and CH_3Hg^+ in the presence of 0.1 mg mL^{-1} of HSA (Fig. 6d and S17†). In both cases, we could observe concentration-dependent changes in absorbance upon the addition of mercury. When the changes in the absorbance ($Abs_{394\ nm}/Abs_{292\ nm}$) values were plotted against the concentration of added CH_3Hg^+ or Hg^{2+}, we could obtain linear plots. This finding indicates that even in the presence of plasma proteins, quantitative estimation of CH_3Hg^+ or Hg^{2+} ion is possible using the present method.

Waste-water management. Poisoning by Hg^{2+} even at a low level results in muscle weakness, skin irritation, breathing problem, poor coordination, *etc.*[23] Therefore, it is important to devise a reliable, low-cost method to check the presence of Hg^{2+} ions in drinking water samples, particularly beyond its permissible levels (*i.e.* 2 ppb). Considering this, here, we have examined water samples collected from three different sources, a tap, a pool, and the Arabian Sea, and we determined the presence of CH_3Hg^+ and Hg^{2+} ions using the current colorimetric method.[23] Before the analysis, the spectra of **1** were recorded in blank water samples to rule out the possibility of background inference. Then, the changes in absorbance were recorded for the samples spiked with Hg^{2+} (0–2 ppm) and CH_3Hg^+ (0–10 ppm) (Fig. S18†). In all the cases, the presence of Hg^{2+} and/or CH_3Hg^+ was also quantified using the atomic absorption spectroscopic technique. Standard equations, as obtained from titration studies, were used for quantitative analysis. A comparison using the AAS method indicated that the recovery values mostly varied from 96% to 103%, whereas the RSDs were found to be less than 4% (Fig. 7c). The small standard deviation values with high percentage recovery indicate fairly good accuracy of the present method.

Low-cost paper strips for on-site detection. It is evident that the regular monitoring of heavy-metal pollutants, such as Hg^{2+} in drinking water and marketed food items, is important for their controlled uptake. However, in most cases, people have no access or means to avail themselves of sophisticated analytical facilities for such diagnoses. Considering this, herein, we have developed test-strips (paper strips coated with compound **1**) for rapid, on-site detection of Hg^{2+}.[24] The paper strips coated with **1** showed no detectable color in normal daylight but showed blue fluorescence under a UV torch. However, the test strips turned yellow in color when exposed to both Hg^{2+} and CH_3Hg^+-contaminated solutions. Similarly, a concentration-dependent quenching of the blue fluorescence intensity was noticed under long UV light. However, unlike Hg^{2+}, the extent of fluorescence quenching was less with CH_3Hg^+ (Fig. 7a). Further, the mercury-mediated change in color (or fluorescence) was quantified using readily available image processing software, ImageJ (Fig. 7b & S19a†). Further, the selectivity experiment was performed by applying the other metal ions onto these test strips under similar conditions (Fig. S19b†). The observations indicate that the present system can sense Hg^{2+} in real-life samples without facing significant interference from other competing metal ions. Further, the

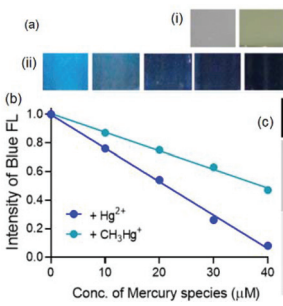

Sample (water)		LOD (ppb)	Recovery (%) (average)	RSD (%)
Hg^{2+} Species	Tap	4.8	98.5 – 102.3	2.96
	Pond	5.7	99.2 – 103.1	3.15
	Sea	6.5	98.7 – 103.6	2.72
CH_3Hg^+ Species	Tap	24.3	99.5 – 102.8	2.53
	Pond	20.8	98.1 – 103.7	3.32
	Sea	32.5	96.8 – 102.9	3.54

Fig. 7 (a) Detection of Hg^{2+} and CH_3Hg^+ (0–40 μM) using test trips (paper strips coated with **1**). Effect of Hg^{2+} under (i) normal daylight and (ii) a UV lamp; (iii) effect of CH_3Hg^+ under a UV lamp. (b) Quantification of FL color change upon addition of Hg^{2+} and CH_3Hg^+ using ImageJ software. (c) Detection of Hg^{2+} and CH_3Hg^+ in different water samples.

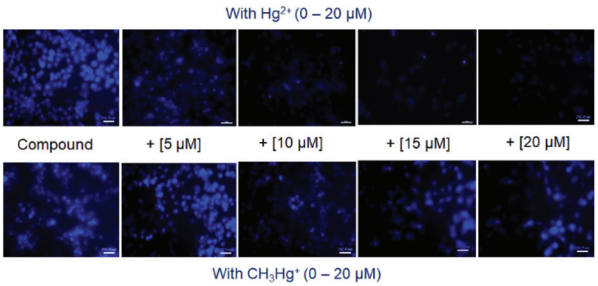

Fig. 8 Intracellular imaging of Hg^{2+} (0–20 μM) (top lane) and CH_3Hg^+ (0–20 μM) (down lane) in HeLa cells using compound **1** (10 μM).

Hg^{2+}-treated paper discs were dipped into EDTA solution, which could effectively leach out the coordinated Hg^{2+} ion, and the paper discs became ready to be reused. Thus, one can even use the same paper disc more than once for the detection of Hg^{2+}. Thus, we can confirm that the present system can also report reversible sensing of Hg^{2+} on a solid surface.

Detection of CH_3Hg^+ and Hg^{2+} under intracellular conditions. Subsequently, compound **1** was employed for detection of Hg^{2+} and CH_3Hg^+ under intracellular conditions in HeLa cells (cervical cancer cell line). To achieve this, we first performed a cell-viability assay (using MTT as the indicator dye) in the presence of **1** (Fig. S20†).[25] No significant reduction in the cell viability was observed even in the presence of ~50 μM **1**, which ensures that **1** can be utilized for the intracellular imaging of mercury species. Dose-dependent kinetic studies suggested that 10 μM of **1** for a 40 min incubation at 37 °C was sufficient for complete cellular uptake. As expected, the cells stained with **1** showed blue-colored fluorescence. Then, the cells (pretreated with **1**) were exposed to both Hg^{2+} (20 μM) and CH_3Hg^+ (20 μM) (Fig. 8). Although quenching of the fluorescence intensity was observed in both cases, the extent of quenching was prominent when the cells were incubated with CH_3Hg^+. These observations indicate that the compound can not only detect Hg^{2+} inside living mammalian cells, but is also able to discriminate between Hg^{2+} and CH_3Hg^+.

Conclusions

Fluorescent nanoaggregates based on a phenanthroline-based amphiphilic probe (**1**) have been utilized for naked-eye sensing of heavy metal pollutants. Addition of both Hg^{2+} (LOD: 4.8 ppb) and CH_3Hg^+ (LOD: 18.2 ppb) induced ratiometric changes in solution color from colorless to yellow. Although quenching of fluorescence intensity was witnessed with both the species, the extent of change was more prominent with Hg^{2+} (~12-fold) than with CH_3Hg^+ (~4-fold). Also, unlike Hg^{2+}, CH_3Hg^+ needs a relatively long incubation period (~10 min). The larger size of CH_3Hg^+ (soft acid) with less charge density might be the reason for this observation. Mechanistic investigation indicates that both Hg^{2+} and CH_3Hg^+ bind with phenanthroline nitrogen ends and facilitate the charge transfer interaction while destabilizing the preformed nanoaggregates. However, **1** could show selective interaction with CH_3Hg^+ when pretreated with EDTA. Then, the probe molecule was utilized to analyze heavy metal pollutants in drinking water and biological samples. The high recovery values (96%–103%) with relatively small standard deviation (<4%) values indicate good accuracy of the present method. Low-cost test strips were designed for rapid, on-site detection. Further, the *in situ* formed metal complex was utilized for sensing of thiol-containing amino acids, such as cysteine (LOD: 6 ppb) and homocysteine (LOD: 5 ppb). Mechanistic investigations indicate that the amino acids can form tertiary complexes with the preformed metal complex (cooperative manner). The compound was utilized for intracellular bioimaging of both Hg^{2+} and CH_3Hg^+ species.

Conflicts of interest

There are no conflicts to declare.

Acknowledgements

The author thanks JSPS (Japan) for a postdoctoral fellowship and BITS-Pilani, Hyderabad for the research initiation grant (RIG) and other technical support. Also, author wish to acknowledge Prof. S. Bhattacharya (Director, IACS) for kind support and encouragement.

Notes and references

1 J. Briffa, E. Sinagra and R. Blundell, *Heliyon*, 2020, **6**, e04691.
2 (*a*) K. P. Carter, A. M. Young and A. E. Palmer, *Chem. Rev.*, 2014, **114**, 4564–4601; (*b*) J. Gu, F. Zhang, Z. Zheng, X. Li, R. Deng, Z. Zhou, L. Ma, W. Liu and Q. Wang, *Chin. Chem. Lett.*, 2021, **32**, 87–91.
3 (*a*) B. Kaur, N. Kaur and S. Kumar, *Coord. Chem. Rev.*, 2018, **358**, 13–69; (*b*) N. Dey and S. Bhattacharya, *Chem. Rec.*, 2016, **16**, 1934–1949; (*c*) N. Dey and S. Bhattacharya, *Chem. – Asian J.*, 2020, **15**, 1759–1779.
4 (*a*) Y. K. Yang, S. K. Ko, I. Shin and J. Tae, *Org. Biomol. Chem.*, 2009, **7**, 4590–4593; (*b*) M. Q. Yang, C. P. Zhou, Y. Chen, J. J. Li, C. H. Zeng and S. Zhong, *Sens. Actuators, B*, 2017, **248**, 589–596; (*c*) S. L. Pan, K. Li, L. L. Li, M. Y. Li, L. Shi, Y. H. Liu and X. Q. Yu, *Chem. Commun.*, 2018, **54**, 4955–4958.
5 (*a*) W. N. Wu, H. Wu, Y. Wang, X. J. Mao, B. Z. Liu, X. L. Zhao, Z. Q. Xu, Y. C. Fan and Z. H. Xu, *RSC Adv.*, 2018, **8**, 5640–5646; (*b*) X. Kong, L. J. Hou, X. Shao, S. M. Shuang, Y. Wang and C. Dong, *Spectrochim. Acta, Part A*, 2019, **208**, 131–139.
6 D. R. Wallace and E. Bates, *J. Clin. Toxicol.*, 2015, **5**, 1000273.
7 L. N. Neupane, J. Park, P. K. Mehta, E. T. Oh, H. J. Park and K. H. Lee, *Chem. Commun.*, 2020, **56**, 2941–2944.

8 (*a*) J. A. Thomas, *Dalton Trans.*, 2011, **40**, 12005–12016; (*b*) Z. Liu, W. He and Z. Guo, *Chem. Soc. Rev.*, 2013, **42**, 1568–1600; (*c*) N. Dey, D. Biswakarma, A. Gulyani and S. Bhattacharya, *ACS Sustainable Chem. Eng.*, 2018, **6**, 12807–12816.

9 (*a*) L. E. Valenti, C. P. D. Pauli and C. E. Giacomelli, *J. Inorg. Biochem.*, 2006, **100**, 192–200; (*b*) G. Agarwal, R. R. Naik and M. O. Stone, *J. Am. Chem. Soc.*, 2003, **125**, 7408–7412.

10 (*a*) P. Mateus and R. Delgado, *Dalton Trans.*, 2020, **49**, 17076–17092; (*b*) D. Kraskouskaya, M. Bancerz, H. S. Soor, J. E. Gardiner and P. T. Gunning, *J. Am. Chem. Soc.*, 2014, **136**, 1234–1237.

11 (*a*) N. Dey and S. Bhattacharya, *Chem. – Eur. J.*, 2017, **23**, 16547–16554; (*b*) N. Dey, *J. Mol. Liq.*, 2021, **327**, 114799.

12 (*a*) N. Kaur, G. Kaur and P. Alreja, *J. Photochem. Photobiol., A*, 2018, **353**, 138–142; (*b*) N. Kaur and P. Alreja, *Tetrahedron Lett.*, 2015, **56**, 182–186.

13 (*a*) N. Dey, S. Bhattacharjee and S. Bhattacharya, *ChemistrySelect*, 2020, **5**, 452–462; (*b*) N. Dey, N. Kumari, D. Biswakarma, S. Jha and S. Bhattacharya, *Inorg. Chim. Acta*, 2019, **487**, 50–57.

14 (*a*) J. H. Hu, J. B. Li, J. Qi and J. J. Chen, *New J. Chem.*, 2015, **39**, 843–848; (*b*) H. Shuai, C. Xiang, L. Qian, F. Bin, L. Xiaohui, D. Jipeng, Z. Chang, L. Jiahui and Z. Wenbin, *Dyes Pigm.*, 2021, **187**, 109125; (*c*) Y. W. Sie, C. L. Li, C. F. Wan, J. H. Chen, C. H. Hu and A. T. Wu, *Inorg. Chim. Acta*, 2018, **469**, 397–401.

15 N. Dey and S. Bhattacharya, *Anal. Chem.*, 2017, **89**, 10376–10383.

16 P. Mahato, S. Saha, P. Das, H. Agarwallad and A. Das, *RSC Adv.*, 2014, **4**, 36140–36174.

17 (*a*) W. N. Wu, H. Wu, Y. Wang, X. J. Mao, B. Z. Liu, X. L. Zhao, Z. Q. Xu, Y. C. Fan and Z. H. Xu, *RSC Adv.*, 2018, **8**, 5640–5646; (*b*) X. Kong, L. J. Hou, X. Shao, S. M. Shuang, Y. Wang and C. Dong, *Spectrochim. Acta, Part A*, 2019, **208**, 131–139.

18 S. Oh, J. Jeon, J. Jeong, J. Park, E. T. Oh, H. J. Park and K. H. Lee, *Anal. Chem.*, 2020, **92**, 4917–4925.

19 D. Wang, X. Zhang, C. He and C. Duan, *Org. Biomol. Chem.*, 2010, **8**, 2923–2925.

20 (*a*) J. M. Jung, C. Kim and R. G. Harrison, *Sens. Actuators, B*, 2018, **255**, 2756–2763; (*b*) Y. W. Choi, J. J. Lee, G. R. You and C. Kim, *RSC Adv.*, 2015, **5**, 38308–38315.

21 (*a*) N. Dey, A. Ali, M. Kamra and S. Bhattacharya, *J. Mater. Chem. B*, 2019, **7**, 986–993; (*b*) N. Dey, N. Kumari, D. Bhagat and S. Bhattacharya, *Tetrahedron*, 2018, **74**, 4457–4465.

22 B. M. W. Fong, T. S. Siu, J. S. K. Lee and S. Tam, *J. Anal. Toxicol.*, 2007, **31**, 281–287.

23 (*a*) H. N. Kim, W. X. Ren, J. S. Kim and J. Yoon, *Chem. Soc. Rev.*, 2012, **41**, 3210–3244; (*b*) G. Li, J. Wang, D. Li, S. Liu, J. Yin, Z. Lai and G. Yang, *Chin. Chem. Lett.*, 2021, **32**, 1527–1531.

24 (*a*) N. Dey, *Analyst*, 2020, **145**, 4937–4941; (*b*) N. Dey, *ChemistrySelect*, 2020, **5**, 6823–6827.

25 A. Chatterjee, M. Banerjee, D. G. Khandare, R. U. Gawas, S. C. Mascarenhas, A. Ganguly, R. Gupta and H. Joshi, *Anal. Chem.*, 2017, **89**, 12698–12704.